A&A 509, A87 (2010)
DOI: 10.1051/0004-6361/200912274

Astronomy & Astrophysics

Radiolysis of ammonia-containing ices by energetic, heavy, and highly charged ions inside dense astrophysical environments

S. Pilling[1,2], E. Seperuelo Duarte[1,3,4], E. F. da Silveira[1], E. Balanzat[3], H. Rothard[3], A. Domaracka[3], and P. Boduch[3]

[1] Departamento de Física, Pontifícia Universidade Católica do Rio de Janeiro (PUC-Rio), Rua Marquês de São Vicente 225, CEP 22453-900, Rio de Janeiro, Brazil
e-mail: sergiopilling@yahoo.com.br
[2] Instituto de Pesquisa & Desenvolvimento (IP&D), Universidade do Vale do Paraíba (UNIVAP), Av. Shishima Hifumi 2911, CEP 12244-000, São José dos Campos, SP, Brazil
[3] Centre de Recherche sur les Ions, les Matériaux et la Photonique (CEA /CNRS /ENSICAEN /Université de Caen-Basse Normandie), CIMAP – CIRIL – GANIL, Boulevard Henri Becquerel, BP 5133, 14070 Caen Cedex 05, France
[4] Grupo de Física e Astronomia, CEFET/Química de Nilópolis, Rua Lúcio Tavares 1052, CEP 2653-060, Nilópolis, Brazil

Received 4 April 2009 / Accepted 20 October 2009

ABSTRACT

Deep inside dense molecular clouds and protostellar disks, interstellar ices are protected from stellar energetic UV photons. However, X-rays and energetic cosmic rays can penetrate inside these regions triggering chemical reactions, molecular dissociation, and evaporation processes. We present experimental studies of the interaction of heavy, highly charged, and energetic ions (46 MeV $^{58}Ni^{13+}$) with ammonia-containing ices H_2O:NH_3 (1:0.5) and H_2O:NH_3:CO (1:0.6:0.4) in an attempt to simulate the physical chemistry induced by heavy-ion cosmic rays inside dense astrophysical environments. The measurements were performed inside a high vacuum chamber coupled to the IRRSUD (IR radiation SUD) beamline at the heavy-ion accelerator GANIL (Grand Accelerateur National d'Ions Lourds) in Caen, France. The gas samples were deposited onto a polished CsI substrate previously cooled to 13 K. In-situ analysis was performed by a Fourier transform infrared spectrometer (FTIR) at different fluences. The average values of the dissociation cross-section of water, ammonia, and carbon monoxide due to heavy-ion cosmic ray analogs are $\sim 2 \times 10^{-13}$, 1.4×10^{-13}, and 1.9×10^{-13} cm^2, respectively. In the presence of a typical heavy cosmic ray field, the estimated half life of the studied species is $2–3 \times 10^6$ years. The ice compaction (micropore collapse) produced by heavy cosmic rays seems to be at least 3 orders of magnitude higher than that produced by (0.8 MeV) protons. The infrared spectra of the irradiated ice samples exhibit lines of several new species including HNCO, N_2O, OCN^-, and NH_4^+. In the case of the irradiated H_2O:NH_3:CO ice, the infrared spectrum at room temperature contains five bands that are tentatively assigned to vibration modes of the zwitterionic glycine ($NH_3^+CH_2COO^-$).

Key words. astrochemistry – methods: laboratory – ISM: molecules – molecular data – molecular processes – cosmic rays

1. Introduction

The birthplace of stars is the densest and coldest place of the interstellar medium (ISM) called dense molecular clouds. These regions have typical gas densities of 10^3–10^8 atoms cm^{-3} and temperatures of the order of 10–50 K. Because of the low temperature, dust particles (mainly silicates and carbonaceous compounds such as amorphous C and SiC) can accrete molecules from the gas phase and become coated with an ice mantle. The interstellar ice mantles (or simply interstellar ices) consist primarily of amorphous H_2O, but usually also contain a variety of other simple molecules such as CO_2, CO, CH_3OH, and NH_3 (e.g., Ehrenfreund & Charnley 2000; Ehrenfreund & Shuttle 2000; Gibb et al. 2001; Boogert et al. 2004). Laboratory studies and astronomical observations indicate that photolysis and radiolysis of such ices can create complex organic compounds, and even prebiotic molecules such as amino acids and nucleobases (e.g., Bernstein et al. 2002; Muñoz Caro et al. 2002; Kobayashi et al. 2008).

The observation of molecules in the gas phase deeply inside these cold and dense regions, where the gas sticking efficiency on grains is close to unity, suggests that they are indeed energetically active regions (e.g., Ehrenfreund & Charnley 2000). Only a negligible amount of stellar UV photons reaches the inner parts of dense regions (Tielens & Hagen 1982; d'Hendecourt et al. 1985). Other mechanisms have therefore been proposed to explain the presence of free molecules such as cosmic-ray-induced UV photons (Prasad & Tarafdar 1983) and direct cosmic ray interaction with ice mantles (e.g. Shen et al. 2004). Both processes lead to molecular desorption from the surface. As pointed out by Shen et al. (2004), in the case of cosmic ray particles, the sputtering produced by direct impact and whole grain heating (classical sublimation) due to energy deposition in the bulk are also two efficient processes for releasing molecules from frozen surfaces to the gas phase.

The first detection of ammonia ices occurred around the for stellar source (YSO) NGC 7538 IRS9 (Lacy et al. 1998). It has also been observed around the massive protostar GCS3 (Chiar et al. 2000) and several other massive YSO such as W33A (Gibb et al. 2000, 2001). Ammonia has also been detected extensively inside the solar system in cometary coma and on several moons (e.g., Kawakita et al. 2006; Bird et al. 1997; Moore et al. 2007, and references therein).

One of the most reactive and important molecules observed from photolysis and radiolysis experiments of ammonia-containing ices, in which there is a carbon source, is the cyanate ion, OCN^- (e.g., Demyk et al. 1998; Hudson & Moore 2000; van Broekhuizen et al. 2005, and references therein). Its infrared

band around 2165 cm^{-1} was observed in several protostellar sources (e.g., Lacy et al. 1984; Gibb et al. 2000; Whittet et al. 2001) indicating regions where UV photochemistry and ion/electron bombardments have played an important role in the chemical alteration of grain mantles.

Although the flux of heavy ions (e.g., Fe, Ni, Si, Mg, ...) is about 3–4 orders of magnitude lower than that of protons (Roberts et al. 2007; Mennella et al. 2003), their effects play an important role on interstellar grains since they can deposit about 100 times more energy than the light ions (He^+ and protons) inside the grains. Brown et al. (1984) and Fama et al. (2008) using high energy He^+ and protons have found that the sputtering yields scales with the square of the electronic stopping power. We demonstrated that this square law extends its validity up to values corresponding to electronic stopping, such as those induced by swift heavy ions (Seperuelo Duarte et al. 2009a,b). Consequently, the number of species released per impact to gas phase due to heavy ions could be 4–5 orders of magnitude higher than for protons.

To characterize the effects of heavy ions on different interstellar ice analogs, it is necessary to measure their sputtering yields and chemical reaction cross-sections and to compare them to those caused by He^+ and protons. Studies of the effect of heavy projectiles in astrophysical ice analogs are scarce. Most experiments have been performed in the keV or hundred of keV range, mainly with protons, He, and Ar ions (e.g., Loeffler et al. 2006; Gomis et al. 2004a,b). Because of the low kinetic energy of these ions, the structural and chemical changes in the frozen ices are mainly governed by nuclear energy loss in elastic ion-target atom collisions (e.g., Brown et al. 1982, 1984).

In this work, we present infrared measurements of ammonia-containing astrophysical ice analogs (H_2O:NH_3 (1:0.5) and H_2O:NH_3:CO (1:0.6:0.4)) irradiated by 46 MeV $^{58}Ni^{13+}$ to simulate the modification induced by heavy cosmic rays inside dense astrophysical environments. At these high ion velocities, the energy deposition is mainly due to inelastic electronic interactions with target electrons (electronic-stopping-power regime).

2. Experimental

We have used the facilities at the heavy ion accelerator GANIL (Grand Accelerateur National d'Ions Lourds) in Caen, France. Briefly, 46 MeV $^{58}Ni^{13+}$ ion projectiles impinge perpendicularly onto the ice target. In this paper, results for two ammonia-containing ices H_2O:NH_3:CO (1:0.5:0.4) and H_2O:NH_3 (1:0.5) are presented. The incoming charge state 13+ corresponds approximately to the equilibrium charge state after several collisions of 46 MeV Ni atoms (independent of the initial charge state) with matter (e.g. Nastasi et al. 1996).

In-situ Fourier-transformed infrared (FTIR) spectra were recorded for ices irradiated at different fluences, up to 2 × 10^{13} ions cm^{-2} using a Nicolet FTIR spectrometer (Magna 550) from 4000 to 650 cm^{-1} with 1 cm^{-1} resolution. The ion flux was 2 × 10^9 cm^{-2} s^{-1}. A background allowing the absorbance measurements is collected before gas deposition. The total irradiation time was about 3 h for each sample. For further experimental details, we refer to Seperuelo Duarte et al. (2009a).

The sample-cryostat system can be rotated 180° and fixed at three different positions to allow: i) gas deposition; ii) FTIR measurement; and iii) perpendicular irradiation as shown in Fig. 1. The thin ice film was prepared by condensation of gases (purity superior to 99%) onto a CsI substrate attached to a closed-cycle helium cryostat, cooled to 12–13 K. A very small

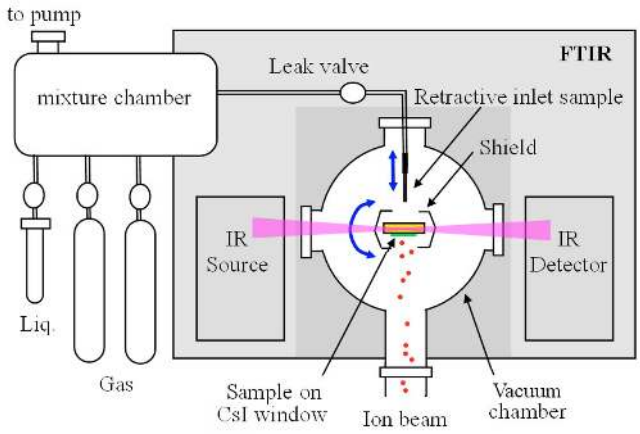

Fig. 1. Schematic diagram of the experimental set-up. The ion beam impinges perpendicularly on the thin ice film deposited on a CsI crystal.

fraction of the mixture CO_2, $CO^{18}O$ and $C^{18}O_2$ existed as contaminants in the pre-chamber. During the experiment the chamber pressure was around 2 × 10^{-8} mbar.

Following d'Hendecourt & Allamandola (1986), the molecular column density of a sample was determined from the relation between optical depth $\tau_\nu = \ln(I_0/I)$ and the band strength, A (cm molec^{-1}), of the respective sample vibrational mode. In this expression, I and I_0 is the intensity of light at a specific frequency before and after passing through a sample, respectively. Since the absorbance measured by the FTIR spectrometer was $Abs_\nu = \log(I_0/I)$, the molecular column density of ice samples was given by

$$N = \frac{1}{A}\int \tau_\nu \mathrm{d}\nu = \frac{2.3}{A}\int Abs_\nu \mathrm{d}\nu \quad [\mathrm{molec\ cm^{-2}}], \tag{1}$$

where $Abs_\nu = \ln(I_0/I)/\ln(10) = \tau_\nu/2.3$.

From these measurements and assuming an average density for the ice samples of about 1 g/cm^3 (water ice), the thickness and the deposition rate are determined. For the H_2O:NH_3:CO ice (1:0.6:0.4) mixture, the thickness was about 1.7 μm and the deposition rate ~13 μm/h. For the H_2O:NH_3 ice (1:0.5), the thickness was ~1.4 μm and the deposition rate was about 10.5 μm/h.

The analyzed ice layers were thin enough: i) to avoid saturation of the FTIR signal in transmission mode; and ii) to be fully crossed by an ion beam of approximately the same velocity. This latter point is important since a relatively low total kinetic energy loss of the projectile in the film guarantees that the studied cross-sections remain constant.

The vibrational band positions and their infrared absorption coefficients (band strengths) used in this work are given in Table 1.

3. Results

Figure 2a, b presents the infrared spectra of H_2O:NH_3:CO ice (1:0.6:0.4) before (highest curve) and after different irradiation fluences. Each spectrum has an offset of 0.05 for clearer visualization. The narrow peak at 2100 cm^{-1} is the CO stretching mode (ν_1). The broad structure from 3100 to 3500 cm^{-1} represents a combination of vibration modes of water (ν_1) and ammonia (ν_1). The band at 1600 cm^{-1} consists of two lines corresponding to the water ν_2 vibration mode (1650 cm^{-1}) and ammonia ν_4 vibration mode (1630 cm^{-1}). The feature around 1100 cm^{-1} is the umbrella vibration (ν_2) mode of ammonia and that at 800 cm^{-1}

Table 1. Infrared absorption coefficients (band strengths) used in the column density calculations for the observed molecules.

Frequency (cm^{-1})	Wavelength (μm)	Assignment	Band strength (A) (cm $molec^{-1}$)	Ref.
2342	4.27	CO_2^a (ν_3)	7.6×10^{-17}	[1]
~2234	4.48	N_2O (ν_3)	5.2×10^{-17}	[2]
~2165	4.62	OCN^- (ν_3)	4×10^{-17}	[3]
2139	4.67	CO (ν_1)	1.1×10^{-17}	[4]
~1100	9.09	NH_3 (ν_2)	1.2×10^{-17}	[5]
~800	12.5	H_2O (ν_L)	2.8×10^{-17}	[4]

[a] $CO^{18}O$ and $C^{18}O_2$ at 2325 and 2309 cm^{-1}, respectively. [1] Gerakines et al. (1995); [2] Wang et al. (2001); [3] d'Hendecourt & Allamandola (1986); [4] Gibb et al. (2004); [5] Kerkhof et al. (1999).

is the libration mode (ν_L) of water molecules. The OH dangling bond (OH db) line at about 3650 cm^{-1} is also observed. This band indicates a high degree of porosity (Palumbo 2006) in this ice mixture and will be discussed later. The region between 2400 to 1200 cm^{-1} is shown in detail in Fig. 2b. We can see the (ν_3) band of newly formed cyanate ion OCN^- at 2160 cm^{-1} and NH_4^+ around 1500 cm^{-1}. Increasing the CO_2 abundance as a function of fluence is mainly due to the following processes (CR symbolized cosmic rays):

$$CO \xrightarrow{CR} C + O \quad (2)$$

$$CO + O \rightarrow CO_2. \quad (3)$$

The variation in the column density of the most abundant molecules observed during the irradiation of H_2O:NH_3:CO ice (1:0.6:0.4) by 46 MeV Ni ions is shown in Fig. 2c as a function of fluence. The column density of water was determined by taking into an account the integrated value of IR absorbance between 1025 cm^{-1} and 800 cm^{-1} (approximately the half left part the IR libration band) and multiplying it by a factor of 2. Since this procedure was performed for all IR spectra, the relative error is expected to be small. In the case of CO_2, the column density is the sum of all its isotopic contributions. For both the $CO^{18}O$ and $C^{18}O_2$ molecules, the value of band strength determined for the ν_3 vibration mode CO_2 at 2342 cm^{-1} (Gerakines et al. 1995) was adopted.

The ammonia and CO abundances seem to have a similar dissociation rates reaching half the initial values at a fluence of about 4×10^{12} ions cm^{-2}. The column density of water is constant, at about 2×10^{18} molecules cm^{-2}, decreasing very slowly as the fluence increases. This is attributed to a persistent deposition of water from the residual gas. This effect was not observed in our previous experiments for pure CO and CO_2 ices (Seperuelo Duarte et al. 2009a,b) and was then apparently related to the deposition of water-containing ices.

The OCN^- abundance increases rapidly, reaching a maximum at a fluence between 1.2 and 1.3×10^{13} ions cm^{-2}. The N_2O production reaches a maximum at around 5×10^{12} ions cm^{-2} and remains constant until the end of irradiation (up to a fluence of 2×10^{13} ions cm^{-2}). As pointed out by Jamieson et al. (2005), N_2O was observed in the radiolysis of N_2-CO_2 ices. They proposed a pathway reaction between N_2 and the oxygen atom coming from the dissociation of CO_2 by 5 keV electrons. N_2O was also reported in both N_2+CO and N_2+CO_2 ice irradiations by 0.8 MeV protons from a Van de Graaff accelerator, performed by Hudson & Moore (2002). We performed additional experiments on N_2-CO (1:1) and NH_3-CO (1:1) ices irradiated by 537 MeV

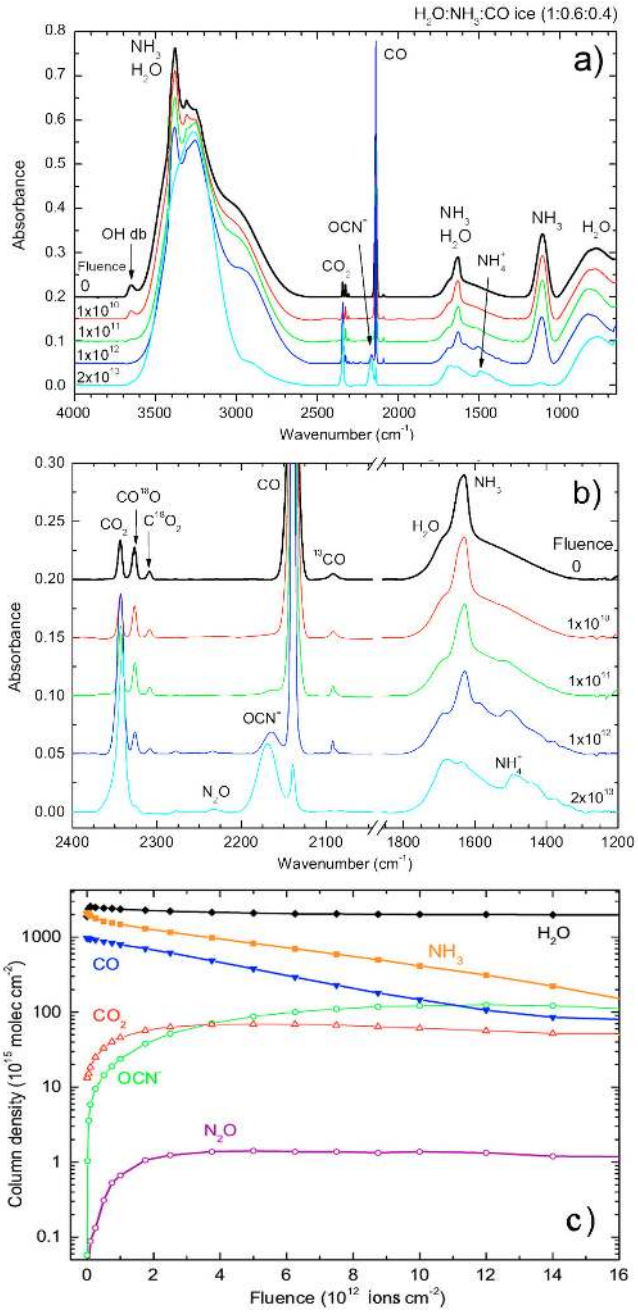

Fig. 2. **a)** Infrared spectra of H_2O:NH_3:CO ice (1:0.6:0.4) before (top dark line) and after different irradiation fluences. **b)** Expanded view from 2400 to 1200 cm^{-1}. Each spectrum has an offset of 0.05 for better visualization. **c)** Molecular column density derived from the infrared spectra during the experiment.

Ni projectiles. N_2O species were observed for the N_2-CO system, confirming the results reported by Jamieson et al. (2005) and by Hudson & Moore (2002), but not for NH_3-CO. The conclusion is that N_2 molecules are not easily formed from NH_3 and that they are required as an intermediate step to synthesize N_2O.

4. Discussion

4.1. Dissociation cross-section

In the present case of fast ions (projectile velocity $\gtrsim$0.2 cm ns^{-1}), most of the deposited energy leads to excitation/ionization of target electrons. In turn, the electrons liberated directly from the

Table 2. Stopping power and penetration depth values for equivelocity 46 MeV ^{58}Ni and 0.8 MeV protons in water ice calculated by SRIM code.

Ion	Stopping Power (keV/μm)		Penetration depth (μm)
	electronic	nuclear	
0.8 MeV p	29	0.02	17.7
46 MeV Ni	4900	15	19.5

inner part of the ion track, about 0.3 nm in diameter for 46 MeV Ni ions (Iza et al. 2006), transfer most of their energy to the surrounding condensed molecules (~3 nm). The re-neutralization of the track proceeds concomitantly with the local temperature rise, leading to an eventual sublimation. At the ice surface, the energy delivered by these heavy ions allows molecules to be removed by sputtering, causing the formation of craters a few nm deep (Schmidt et al. 1991). The sputtering yield, Y, scales with the square of the electronic stopping power inside the target, $S_e = dE/dx$ (e.g., Brown et al. 1984; Famà et al. 2008; Seperuelo Duarte et al. 2009a,b).

In Table 2 we provide the electronic and nuclear stopping power values for 46 MeV ^{58}Ni and its equivelocity protons (0.8 MeV protons) in water ice (ρ = 1 g cm^{-3}), calculated by SRIM[1] – Stopping and Ranges of Ions in Matter code (Ziegler & Biersack [2]). The penetration depths of the particles in the water ice are also shown. The electronic stopping power is at least 2 orders of magnitude higher than the nuclear one; the total stopping power for 46 MeV Ni atoms is about 2 orders of magnitude higher than that of equivelocity protons.

The variation in the molecular abundance due to the incoming radiation can be attributed to several processes: i) the molecular dissociation quantified by the dissociation cross-section, σ_d (cm^2); ii) the sputtering yield, Y (molecules desorbed per ion impact); iii) the formation of molecules, σ_f (cm^2), from species already present as well as from radical and ionic fragments; iv) the molecular layering, L (molecules deposited per ion impact), caused by deposition of the residual gas or the eventual recondensation of sputtered molecules. The layering yield, L, is expressed in terms of molecules deposited by ion impact; it is obtained by dividing the layering rate (molec s^{-1}) by the ion projectile flux (2×10^9 ions s^{-1}).

Taking into account the two "formation" processes (chemical reaction and layering), as well as the two "disappearance" processes (molecular dissociation and sputtering), the column density rate of each molecular species is given by

$$\frac{dN_i}{dF} = \sum_{j \neq i} \sigma_{f,ij} N_j + L_i - \sigma_{d,i} N_i - Y_i \Omega_i(F), \quad (4)$$

where $\sum_j \sigma_{f,ij} N_j$ represents the total molecular production rate of the i species directly from the j species, Y_i is the sputtering yield of a pure ice formed by i species, and $\Omega_i(F)$ is the relative area occupied by the i species on the ice surface.

Assuming: i) that only $i = 1$ species (e.g., water) of the residual gas are able to condense onto the sample (i.e., $L_i = L_1 \delta_{i1}$, where δ_{ij} is the Dirac function); and ii) that the analyzed molecular species cannot react in a one-step process to form another species originally present in the ice (i.e., $\sigma_{f,ij} \approx 0$), this equation system becomes

$$\frac{dN_i}{dF} = -\sigma_{d,i} N_i - (Y_i \Omega_i(F) - L_1 \delta_{i1}). \quad (5)$$

[1] http://www.srim.org

[2] www.srim.org

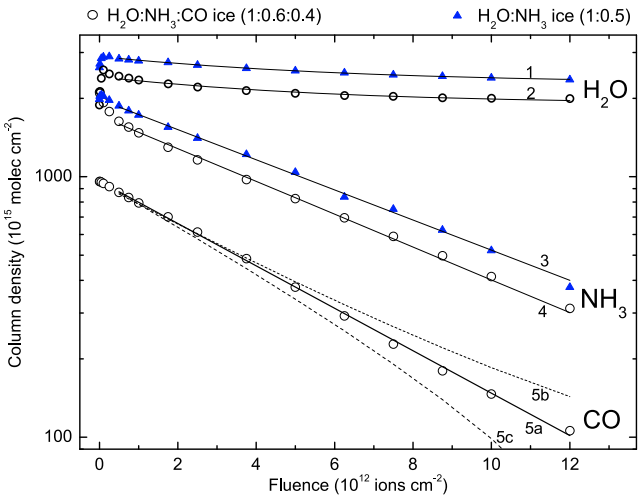

Fig. 3. Variation in the column density of water, ammonia, and CO as a function of fluence. Solid lines represent the best-fit relations using Eqs. (6) and (7). Triangles and circles correspond to different ice samples. Model parameters are listed in Table 3.

As shown in Figs. 3 and 4a (hashed region), there is a non-exponential decreasing behavior at the beginning of the irradiation, whose boundary is defined by $F < F_{min} \approx 5 \times 10^{11}$ ions cm^{-2}. This suggests that ice compaction is occurring, as we later discuss.

Another phenomenon that can also occur is the layering of species 1 over the ice surface ($\Omega_i(F) \to \delta_{i1}$), preventing progressively sputtering of $i \neq 1$ species. At the end of these processes, the equation system in Eq. (5) is decoupled and can be solved analytically to be

$$N_i = N_{0i} \exp(-\sigma_{d,i} F), \quad \text{for } i \neq 1 \text{ species}, \quad (6)$$

and

$$N_1 = (N_{01} - N_{\infty,1}) \exp(-\sigma_{d,1} F) + N_{\infty,1}, \quad (7)$$

where $N_{\infty,1} = (L_1 - Y_1)/\sigma_{d,1}$ is the asymptotic value of column density at higher fluences due to the presence of layering, and N_i and N_{0i} are the column densities of species i at a given fluence and at the beginning of the experiment, respectively. Equation (7) describes the condensation of $i = 1$ species during irradiation. This equation is particulary useful for species that are adsorbed onto the walls of a vacuum chamber as in the case of water, generating a continuous flow towards the cold target, where it creates a superficial layer during the experiment.

Figure 3 presents the best-fit relations of the infrared data for the ices H_2O:NH_3:CO and H_2O:NH_3, derived by employing Eqs. (6) and (7) to describe the column density evolution with the fluence. The condition $\sigma_{f,1j} \approx 0$ applied for water means that the production rate of water molecules from ammonia and carbon monoxide is negligible compared to the layering rate. Since $F_{min} \approx 5 \times 10^{11}$ ions cm^{-2} for the current data, the fit cover only the $F = 1{-}12 \times 10^{12}$ ions cm^{-2} range to avoid both the afore mentioned transient effects and eventual large inhomogeneities in the ice induced at too large fluences. The observed decrease in N_i for CO and NH_3 ices is indeed exponential, leading to the CO dissociation cross-section of value 1.9 $\times$ 10^{-13} cm^2, in agreement with the value obtained for pure CO ice irradiated by the same projectiles (Seperuelo Duarte et al. 2009b). The values for NH_3 are 1.3 and 1.4$\times$10^{-13} cm^2, obtained with the H_2O:NH_3 and H_2O:NH_3:CO ice, respectively. The fitting parameters (dissociation cross-section, sputtering, layering, and the initial relative

Table 3. Dissociation cross-sections of the studied molecular species for radiolysis of ammonia-containing ices by 46 MeV Ni ions.

Species	Mixture (H_2O:NH_3:CO)	σ_d (10^{-13} cm^2)	N_∞ (10^{17} molec cm^{-2})	Y (10^4 molec ion^{-1})	L^f (10^4 molec ion^{-1})	N_0 (10^{17} molec cm^{-2})	Model
H_2O	(1:0.5:0)	~2	23	1[a]	38	29	1
	(1:0.6:0.4)	~2	19	1[a]	35	24	2
NH_3	(1:0.5:0)	1.3	NA[e]	0[b]	0	2.0	3
	(1:0.6:0.4)	1.4	NA	0[b]	0	1.7	4
CO	(1:0.6:0.4)	1.9	NA	0[b]	0	1.0	5a
	(1:0.6:0.4)	1.9	NA	0[b]	1[d]	1.0	5b
	(1:0.6:0.4)	1.9	NA	1[c]	0	1.0	5c

[a] Taken from Brown et al. (1984); [b] no sputtering. Assuming that the water layering is thick enough to fully cover the NH_3 or CO molecules on the surface; [c] assuming that there is no water layering and considering a sputtering of 1×10^4 molec ion^{-1} (the same adopted for water molecules), [d] assuming an extra source of CO for layering; [e] NA=Not applied; [f] for H_2O: derived from $L = N_\infty \sigma_d + Y$. For NH_3 and CO: assuming no layering (except model 5b).

molecular abundance of each species in the ices) are listed in Table 3. The individual effects of layering or sputtering on the column density (e.g., for CO species) correspond to the models 5b and 5c, respectively.

The H_2O column density data, presented in Fig. 2c, level off around 2×10^{18} molec cm^{-2} for the two samples. The average value for the dissociation cross-section of water, employing Eq. (6), is $\sigma_{d,1} \sim 2 \times 10^{-13}$ cm^2. The sputtering yield for water measured by Brown et al. (1984) was extrapolated for the 46 MeV Ni ions impact by using the stopping power given in Table 2. The obtained value is $Y_1 = 1 \times 10^4$ molecules per impact, and the estimated average water layering of both experiments is 4×10^5 molec ion^{-1}, obtained from the relation $L = N_\infty \sigma_d + Y$. Because of the high value of water layering, the NH_3 and CO species were recovered by a H_2O film during irradiation and their sputtering yields were considered to be negligible; therefore, the data were adjusted directly by Eq. (6).

4.2. Ice compaction

A high density amorphous form of water ice is found when water vapor is deposited onto very cold ($T < 30$ K) surfaces, at a rate of <100 μm/h (Jenniskens et al. 1998). Both of our experiments are within this regime. Nevertheless, the ice mixture containing CO was found to be less compact than the H_2O:NH_3 ice. This conclusion is consistent with the observation of large changes in the column density of the adsorbed species (Fig. 4a) and is supported by the presence of the OH dangling bond (OH db) line around 3650 cm^{-1} (Fig. 4b), which is attributed to water molecules in the surfaces of micropores (Rowland & Devlin 1991; Rowland et al. 1991; Palumbo 2006, and references therein). Since both ices were deposited roughly at the same rate (~12 μm/h) and at the same temperature (~13 K), the porosity enhancement must be produced by CO molecules, which diffuse very efficiently into the ice (e.g., Collings et al. 2004). Some cavities are eventually created during the ice formation reducing its compaction.

Figure 4a presents an expanded view of Fig. 3 corresponding to fluences of up to 3.5×10^{12} ions cm^{-2}, i.e., at the beginning of the irradiation. The hatched region ($F < F_{min}$) indicates the fluences for which the column densities have a complex behavior. These rapid variations, observed for both water and ammonia species, are enhanced in the case of a H_2O:NH_3:CO mixture but are not seen in the CO column density. This may be associated with changes in the band strength of the vibration modes of hydrogen-bound molecules produced by compaction effects at the beginning of the irradiation.

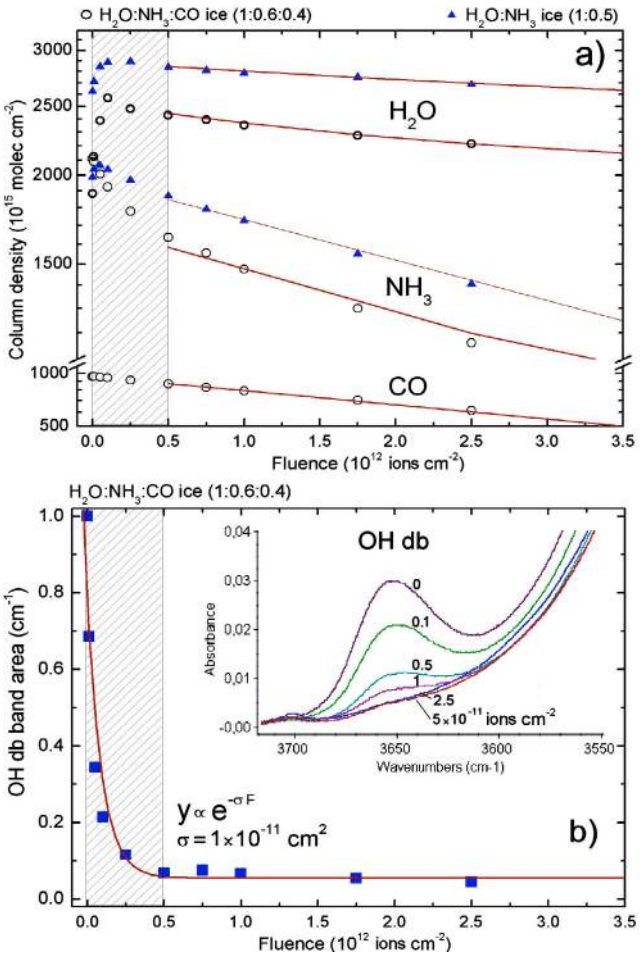

Fig. 4. **a)** Expanded view of Fig. 3 at the beginning of irradiation. Note the drastic changes in column density of water and ammonia up to fluence of 5×10^{11} ions cm^{-2}. The hashed area indicates the regions where compaction is occurring. **b)** OH dangling bond feature area (cm^{-1}) in the H_2O:NH_3:CO ice (1:0.6:0.4) as a function of fluence. Figure inset is the OH db feature from non irradiated ice and at fluences 0.1, 0.5, 1, 2.5 and 5×10^{11} ions cm^{-2}.

Direct evidence of the compaction (micropore collapse) caused by the impinging heavy ions is shown in Fig. 4b, where the intensity of the OH db band as a function of fluence is examined. The experimental data (band area, y) were fitted by the exponential curve $y \propto e^{-\sigma F}$, where F is the ion fluence (ions cm^{-2}) and $\sigma = 1 \times 10^{-11}$ cm^2 is the disappearance cross-section. The

estimated error is within 30%. The figure inset presents the OH db feature at 3650 cm^{-1} during the beginning of the irradiation. The traces correspond to fluences 0 (non-irradiated), 0.1, 0.5, 1, 2.5, and 5×10^{11} ions cm^{-2}. The peculiar changes in the column density, at the beginning of the irradiation, and that the OH db feature seems to disappear approximately at the same fluence, around 5×10^{11} ions cm^{-2}, indicate that at this point the ice is fully compacted by the Ni ion beam.

A detailed investigation of the compaction effects of ion bombardment was performed by Palumbo (2006) using 200 keV protons in water-rich ices at 15 K. The intensity of the OH db line was found to decrease after ion irradiation and the amount of absorbed carbon monoxide (from an upper layer of CO ice) also decreases as the fluence of impinging ions increases. These results indicate that the porosity of amorphous water ice decreases after ion irradiation. Palumbo (2006) quantified the compaction degree of water ice irradiated by 200 keV protons by fitting an exponential function to the integrated area of the OH db peak at different fluences obtaining a "disappearing" cross-section of 4.13×10^{-14} cm^2. Comparing the cross-section of both experiments, compaction effects caused by to heavy and energetic ions (46 MeV Ni ions) are 3 found to be orders of magnitude higher than those produced by (0.8 MeV) protons.

4.3. Synthesis of molecules

4.3.1. Cyanate ion, OCN$^-$

The 2165 cm^{-1} (4.62 μm) peak, commonly referred to the as "XCN" band, was first detected toward the massive protostar W33A (Soifer et al. 1979). Its presence was the first observational indication that complex chemistry (triggered by UV/X-ray photons or ion/electron bombardments) could occur in the interstellar ice mantles. To date, this feature has already been observed in more than 30 deeply embedded mostly high-mass young stellar objects (Tegler et al. 1993; Demyk et al. 1998; Pendleton et al. 1999; Gibb et al. 2000; Keane et al. 2001; van Broekhuizen et al. 2005; Pontoppidan et al. 2003; Whittet et al. 2001; Gibb et al. 2004) and several Galactic center sources (Chiar et al. 2000; Spoon et al. 2003).

The "XCN" band has been studied extensively in the laboratory, being easily produced by proton irradiation (e.g., Moore et al. 1983; Hudson et al. 2001), vacuum ultraviolet photolysis (e.g., van Broekhuizen et al. 2005; Lacy et al. 1984; Grim & Greenberb 1987; Demyk et al. 1998), or thermal annealing of interstellar ices analogues (Raunier et al. 2003; van Broekhuizen et al. 2004). Through the years, several candidates have been proposed to justify the XCN band, including some isonitriles (X-N≡C) and cyanates (X-O-C≡N) (see Pendleton et al. 1999, for review). However, laboratory experiments involving isotopic substitution have proven unequivocally that the agent producing the 2165 cm^{-1} feature is the cyanate ion, OCN$^-$ (Schutte & Greenberg 1997; Bernstein et al. 2000; Novozamsky et al. 2001; Palumbo et al. 2000).

The present work is the first report on the OCN$^-$ formation by heavy, highly charged, and energetic ions (46 MeV ^{58}Ni^{13+}) in an attempt to simulate the chemistry and the physical chemistry induced by cosmic rays inside dense regions of the interstellar medium such as dense molecular clouds or protoplanetary disks.

Following Hudson et al. (2001), a possible route for the production of OCN$^-$, from the radiolysis of interstellar ice analogues, occurs via the reaction of NH or NH_2 radical with CO, leading to the formation of the isocyanic acid molecule HNCO

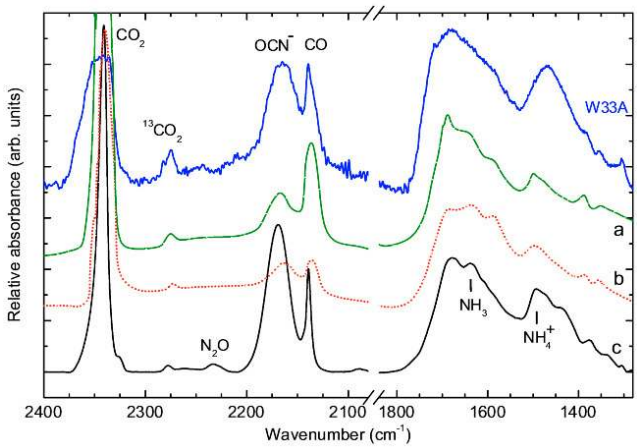

Fig. 5. Comparison between IR spectra of interstellar and laboratory ices. The highest curve is the infrared spectra of protostellar source W33A obtained by the Infrared Space Observatory (ISO). Lower traces indicate laboratory spectra of H_2O:NH_3:CO ices after processing by: **a)** UV photons (Hudson & Moore 2000); **b)** 0.8 MeV protons (Hudson & Moore 2000), and **c)** 46 MeV Ni ions (this work).

$$NH_3 \xrightarrow{CR} (NH_3^+ + e^-) \text{ or } (NH_2 + H) \quad (8)$$

$$NH_3 + NH_3^+ \rightarrow NH_4^+ + NH_2 \quad (9)$$

$$NH_2 + CO \rightarrow H + HNCO \quad \text{or} \quad NH + CO \rightarrow HNCO. \quad (10)$$

The reaction between isocyanic acid and ammonia (by means of acid-base reaction) produces ammonium, NH_4^+, and OCN$^-$, i.e.,

$$HNCO + NH_3 \rightarrow NH_4^+ + OCN^-. \quad (11)$$

In the infrared spectra of the irradiated ices by heavy ions, beyond the OCN$^-$ band, the HNCO and NH_4^+ species are also observed at frequencies of around 2265 and 1490 cm^{-1}, respectively.

A comparison between the infrared spectra of interstellar ices around the embedded protostar W33A with irradiated ammonia-water-CO mixtures from laboratory is given in Fig. 5. The uppermost curve presents the IR spectrum recorded by the Infrared Space Observatory (ISO) toward the protostellar object W33A. The data were extracted from the ISO database[3]. Curve (a) shows the IR spectrum of H_2O:NH_3:CO (1:0.2:0.2) ice at 15 K after 10 min of UV photons from a hydrogen-discharge lamp (Hudson & Moore 2000). Curve (b) presents the IR spectrum of H_2O:NH_3:CO (1:0.2:0.2) ice at 15 K irradiated by 0.8 MeV protons of dosage 19 eV molec^{-1} (Hudson & Moore 2000). The lowest curve (c) shows the infrared spectrum of H_2O:NH_3:CO (1:0.6:0.4) ice at 13 K observed after the bombardment by 46 MeV Ni ions at fluences around 2×10^{13} ions cm^{-2} (this work). The radiolysis of H_2O:NH_3:CO performed by the present study, using heavy and energetic cosmic rays, reproduces very well the OCN$^-$ (2165 cm^{-1}) and CO (2139 cm^{-1}) infrared features observed in the W33A spectrum. Other spectral features such as the broad IR peaks observed at 1650 and 1450 cm^{-1} are also similar to those of the astronomical source.

[3] http://iso.esac.esa.int/ida

4.3.2. Ammonium, NH_4^+

The broad ν_4 vibration mode of NH_4^+ around 1490 cm^{-1} is also observed after the heavy ion bombardment of both ammonia-containing ices (see Figs. 2a,b). This line has also been observed from similar irradiation experiments involving photolysis and radiolysis of ammonia-containing ices (e.g., Demyk et al. 1998; Hudson et al. 2001; Hudson & Moore 2000). As discussed by Demyk et al. (1998), the band strength of the NH_4^+ ν_4 line is very uncertain (because of the broad profile in the astrophysical ice analogs). This, combined with a possible contamination from other infrared lines, makes this particular column density determination very imprecise.

The NH_4^+ formation directly from the processing of ammonia is given by Eqs. (8) and (9). The reaction pathways due to the processing of H_2O:NH_3:CO ice are given by Eqs. (10) and (11). As discussed by Moore et al. (2007), the presence of water in interstellar ices also contributes to convert NH_3 into NH_4^+:

$$H_2O \xrightarrow{CR} H_2O^+ + e^- \quad (12)$$

$$H_2O^+ + H_2O \rightarrow OH + H_3O^+ \quad (13)$$

$$H_2O^+ + NH_3 \rightarrow OH + NH_4^+ \quad (14)$$

$$H_3O^+ + NH_3 \rightarrow H_2O + NH_4^+. \quad (15)$$

Besides the observation of the OCN^- ion, the occurrence of ammonium in several protostellar disks was also observed (Gibb et al. 2000; Boogert et al. 2004; Gibb et al. 2004; Demyk et al. 1998, and references therein) and possibly for several solar system ices (Moore et al. 2007). Following Muñoz Caro & Shutte (2003), NH_4^+ is one of the species involved in the formation of highly complex molecules such as hexamethylenetetramine HMT, $(CH_2)_6N_4$, observed in experiments involving UV photoprocessing of interstellar ammonia-containing ice analogs.

4.3.3. Other species

The infrared spectra of H_2O:NH_3:CO ice (1:0.6:0.4) from 2400 to 1200 cm^{-1} acquired during the slow sample heating, from 13 K up to room temperature, are shown in Fig. 6a. For each spectrum, the sample temperature is indicated. The spectra have an offset of 0.02 for clearer visualization. The CO line at 2139 cm^{-1} decreases drastically at a temperature of between 13 and 52 K. At 150 K, the N_2O peak (~2234 cm^{-1}) increases slightly. The unidentified feature around 1450 cm^{-1} is not seen anymore above this temperature. At 200 K, all the water, ammonia and CO_2 ices have been sublimated and their peaks have disappeared. Although very attenuated, the OCN^- peak (~2169 cm^{-1}) is still present at 200 K. At this temperatures and higher, we observe the appearance of new unidentified line around 2147 cm^{-1} (between the OCN^- and CO peaks). This peak is tentatively assigned to aliphatic isocyanide R-N≡C molecules (2150 cm^{-1}) as observed by Imanaka et al. (2004) in UV photolysis of N_2:CH_4 ices.

A comparison between the irradiated ice at 13 K and the organic residue at 300 K is shown in Fig. 6b. Tentative band attribution is indicated. At room temperature, a large structure (possibly two overlapping peaks) is observed around 2210 cm^{-1}. Since these features are close to the C-N stretch vibration band, we suggest that they may be due to organic residues containing CN-bearing molecules. Vertical dashed lines indicate the possible frequency of some vibration modes of the zwitterionic glycine ($NH_3^+CH_2COO^-$).

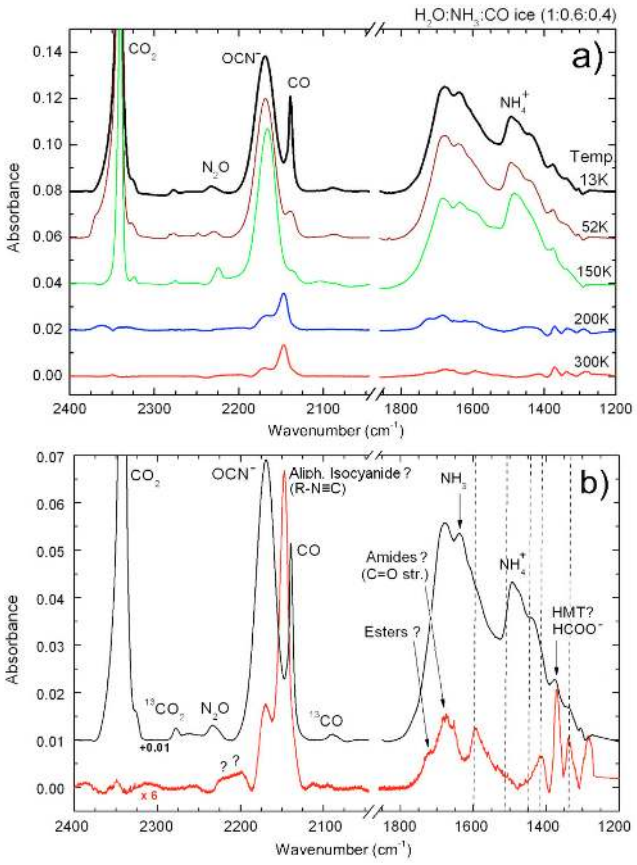

Fig. 6. a) Infrared spectra of H_2O:NH_3:CO ice (1:0.6:0.4) from 2400 to 1200 cm^{-1} during heating to room temperature. The sample temperature of each spectrum is given. Each spectrum has an offset of 0.02 for clearer visualization. **b)** Comparison between the irradiated ice at 13 K (top spectrum) and the 300 K residue (bottom spectrum). Vertical dashed lines indicate the frequencies of some vibration modes of zwitterionic glycine ($NH_3^+CH_2COO^-$).

The observed infrared bands produced by the radiolysis of the H_2O:NH_3:CO ice (1:0.6:0.4) at 13 K by heavy, charged, and energetic ions in the 2400 to 1200 cm^{-1} range are listed in Table 4. The lines observed after the sample heating to room temperature are also shown. The assignments are proposed by comparing the spectra with those of similar experiments by photolysis or radiolysis of interstellar ice analogs (Hudson et al. 2001; Jamieson et al. 2005; Hudson & Moore 2000; van Broekhuizen et al. 2005; Munoz Caro & Shutte 2003; Holtom et al. 2005; Demyk et al. 1998; Imanaka et al. 2004). The low frequency lines are tentatively assigned to N_xO_y molecules (Jamieson et al. 2005).

At room temperature, the peaks around 1593, 1506, 1415, and 1338 cm^{-1} may possibly be assigned to different vibration modes of zwitterionic glycine ($NH_3^+CH_2COO^-$). This amino acid was observed among the residues of the 5 keV electron bombardment of CH_3NH_2:CO_2 (30:1) ice (Holtom et al. 2005) at 10 K. Zwiterionic glycine was also observed after irradiation of NH_3:CH_3COOD (1:1) ice by low energy electrons (Lafosse et al. 2006) at 25 K. These authors observed zwitterionic glycine even at 25 K, without any subsequent thermal activation.

The presence of amino acid precursors has been detected among the organic residues created by the photolysis and radiolysis of several ammonia-containing interstellar ice analogs. The investigation employed vacuum ultraviolet photons from synchrotron light sources (Chen et al. 2008; Nuevo et al. 2007;

Table 4. Assignment of infrared absorption features produced by the radiolysis of the H_2O:NH_3:CO ice (1:0.6:0.4) by 46 MeV Ni ions at 13 K and after warming to 300 K.

Frequency (cm^{-1})	Wavelength (μm)	Temp. (K)	Molecule	Notes
2233	4.48	13	N_2O	[1,2]
2218–2200	4.51-4.54	300	nitriles†	[8]
2168	4.61	13, 300	OCN^-	[1,3,4,7]
2147	4.66	300	aliph. isocyanide†	[8]
~2112	4.73	300	$NCO_2^\dagger$	[2]
1725	5.80	300	ester†	[5]
1683	5.94	300	amides†	[5]
1652	6.05	300	asym-$N_2O_3^\dagger$	[2]
1637	6.11	13	?	
1593	6.28	300	$NH_3^+CH_2COO^{-\dagger}$	[6]
1558	6.42	300	?	
1533	6.52	300	?	
1506	6.64	300	$NH_3^+CH_2COO^{-\dagger}$	[6]
~1490	6.71	13	NH_4^+	[1,3,7]
1474	6.78	13	$NO_3^\dagger$	[2]
1440	6.94	13	$NH_3^+CH_2COO^{-\dagger}$	[6]
1415	7.07	300	$NH_3^+CH_2COO^{-\dagger}$	[6]
~1370	7.30	13, 300	HMT†	[5]
			$HCOO^-$	[5,9]
~1338	7.47	13, 300	$NH_3^+CH_2COO^{-\dagger}$	[6]
			$NH_2CH_2COO^{-\dagger}$	[6]
			$HCOO^-$	[9]
1305	7.66	13	$N_2O_3^\dagger$; $N_2O_4^\dagger$	[2]
1283	7.80	300	$N_2O^\dagger$	[2]

†Tentative assignment. [1] Proton bombardment of several ices (Hudson et al. 2001); [2] Electron bombardment of N_2:CO_2 (Jamieson et al. 2005); [3] Hudson & Moore (2000; [4] van Broekhuizen et al. 2005; [5] UV photolysis of H_2O:NH_3:CH_3OH:CO:CO_2 ice (Munoz Caro & Shutte 2003); [6] electron bombardment of CH_3NH_2:CO_2 ice (Holtom et al. 2005); [7] UV photolysis of ammonia-containing ices (Demyk et al. 1998); [8] UV photolysis of N_2:CH_4 ices at various pressures (Imanaka et al. 2004); [9] proton bombardment of H_2O:NH_3:CO ice (Hudson & Moore 2001).

Nuevo et al. 2006), hydrogen UV-lamp (Elsila et al. 2007; Muñoz-Caro & Schuttle 2003; Bernstein et al. 2002; Muñoz caro et al. 2002), and by ion bombardment (Takano et al. 2007; Kobayashi et al. 2008).

The IR peak centered around 1370 cm^{-1} observed in both 13 K and 300 K spectra was tentatively assigned to hexamethylenetetramine – HMT, $(CH_2)_6N_4$, since a similar feature was also observed in the UV photolysis of H_2O:NH_3:CH_3OH:CO:CO_2 ice by Muñoz Caro and Shutte (2003). The observation of NH_4^+ in the same organic residue reinforces the evidence for HMT, since the ammonium is an essential component of its formation.

The presence of these complex molecules in the organic residue produced by the bombardment of interstellar ice analogs by energetic and heavy ions, has to be confirmed. However, the result of this experiment suggests that even deep inside molecular cores or other dense regions such as protoplanetary disks, the interstellar grains are being transformed significantly . The organic molecules produced, trapped into and onto dust grains, meteoroids, and comets, could be delivered into the planets/moons possibly allowing prebiotic chemistry to take place in these environments where water is also found in liquid state.

4.4. Astrophysical implication

Inside dense regions of the interstellar medium, where direct stellar UV is extremely attenuated, X-rays (despite some degree of attenuation) and cosmic rays are the main drivers of the gas phase and grain surface chemistry. For example, the penetration depth of 46 MeV Ni ions and equivelocity protons inside water ice is about 1 and 3 orders of magnitude higher than for 500 and 50 eV photons (considering the photoabsorption cross-section from Chan et al. (1993) and McLaren et al. (1987), respectively). In these environments, the dust grains can reach a size of the order of a micron, as a coagulation of sub-micron grains occurs with ice-rich mantles of tens of nanometers (Mathis 1990; Mathis, et al. 1977; Li & Greenberg 1997; Chokshi, et al. 1993). However, the presence of larger grains (radii of within one to tens of microns) has also been suggested (Witt et al. 2001; Taylor Baggaley & Steel 1996; Grün et al. 1994).

Figure 7 illustrates, as a schematic view, the interaction between heavy-ion cosmic rays and a typical interstellar grain inside dense clouds. The ion track (along with the coagulated submicron size grains), the grain mantles, the processed material, and the sputtered molecules are indicated. The inset of the figure was adapted from Andrade et al. (2008) and shows the different stages timescales) of physico-chemical changes on the grain mantle caused by the heavy-ion impact. At the pertinent heavy-ion velocities, the projectile traverses atomic distances of the grain mantle in 10^{-17} s. The energetic cosmic-ray analog ionizes and excites molecules along its trajectory inside the solid (inset Fig. 7a). The secondary electrons (δ) move away from the projectile trajectory, generating a positive infratrack in the center and a negative ultratrack around. Afterwards, molecular dissociations and chemical reactions occur, causing the sputtering of light ions such as H^+ (inset Fig. 7c). Following Iza et al. (2006), the sputtering occurs mainly due to long-lived repulsive electronic excitation that leads to atomic or molecular motion.

After the Coulomb repulsion of ionizing species, the next stage is the track relaxation, when preformed or newly formed larger chemical species (molecular clusters) are desorbed (inset Fig. 7d) on timescales of around $\sim 10^{-10}$ s. Shocks transfer momentum to material at the ice surface, promoting molecular desorption from a site located as far as 3–5 nm of the ion track.

Because of the high porosity of grains inside dense clouds (coagulated from sub-micron heterogenic grains), some sputtered species inside the grain pores become confined, being re-adsorbed onto the grains at a later time. The re-adsorption of sputtered species (processed or not) my also occur in the outer layer of the micron-size grain mantle. The projectile energy deposited along the interfaces between the water-rich mantle and the silicate/carbon grain may promote chemical mixing within these two different chemical regions.

Inside dense interstellar regions, the 1 MeV proton flux is around 1 proton $cm^{-2}\,s^{-1}$ (Mennella et al. 2003; Morfill et al. 1976). Inside these regions, the iron-to-proton ratio is about 1.6×10^{-4}, and the iron fraction of the canonical cosmic ray flux is estimated to be 2×10^{-3} $cm^{-2}\,s^{-1}$ (Roberts et al. 2007; Léger et al. 1985). Following Drury et al. (1999), heavy ions with $12 \lesssim Z \lesssim 29$ (e.g., from Mg to Cu) have roughly the same abundance, while those with $Z > 30$ are more than 3 orders of magnitude less abundant. The average cosmic-ray flux consisting of heavy nuclei ions ($Z \gtrsim 12$) is estimated to be $\phi_{\rm HCR} \sim 5\times10^{-2}\,cm^{-2}\,s^{-1}$. Despite this small value, the sputtering produced by heavy and energetic ions can be more than 4 orders of magnitude higher than produced by the more abundant low-energy protons (Léger et al. 1985; Seperuelo Duarte et al. 2009a,b). In regions where

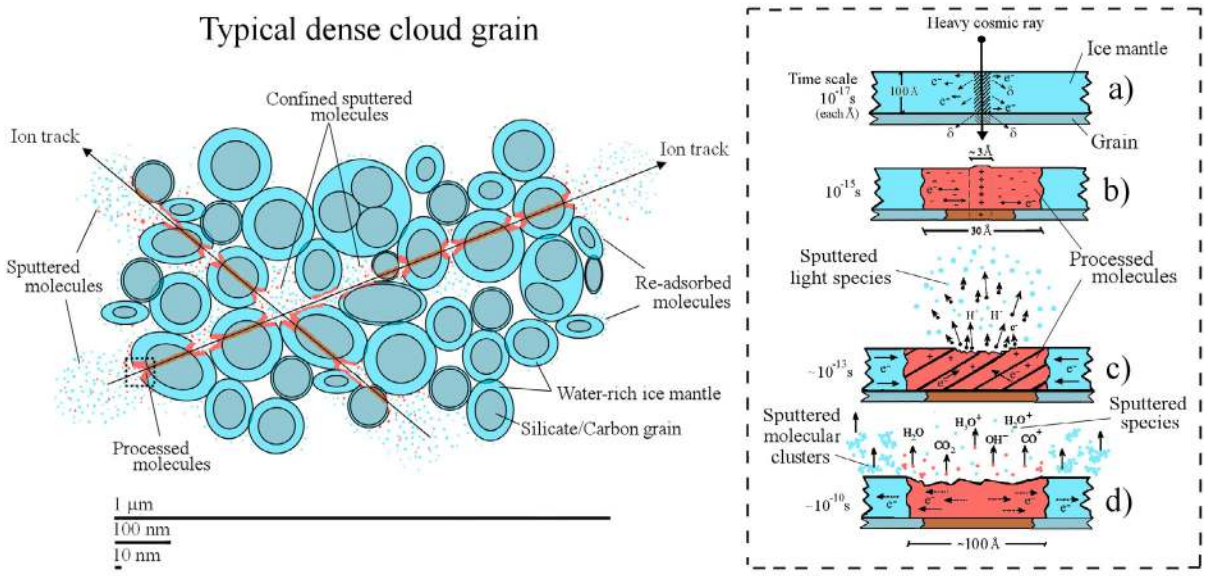

Fig. 7. Schematic view showing the interaction between a heavy-ion cosmic ray and a typical interstellar grain inside dense clouds. The ion track along the coagulate sub-micron size grains, the grain mantles, the processed and the sputtered molecules are indicated. Figure insets were adapted from Andrade et al. (2008) and indicate the physical-chemical changes on the grain mantle due to the impact of a heavy ion. See details in text.

Table 5. Average dissociation rate (R) and the corresponding half-life ($t_{1/2}$) of water, ammonia, and CO molecules under bombardment by 46 MeV Ni ions.

Species	Relative initial abundance	R (10^{-15} s^{-1})	$t_{1/2}$ (10^6 years)
H_2O	50%	8	2
NH_3	30%	7	3
CO	20%	9	2

the ionizing stellar photons are very attenuated, the sputtering caused by cosmic rays also becomes a competitive desorption process. This issue should be taken into consideration in future chemical models of the inner regions of molecular clouds, where a considerable fraction of excited molecules are released into the gas phase by heavy ion impact.

A rough estimation of the half-lives of molecular species in space can be carried out by considering only the molecular dissociation effects of cosmic rays. The average dissociation rate, R, of a given species i, induced by the interstellar heavy cosmic-ray field is approximately given by

$$R_i \approx \phi_{\rm HCR} \times \sigma_{{\rm d},i} \quad [{\rm s}^{-1}], \tag{16}$$

where $\sigma_{{\rm d},i}$ is the average dissociation cross-section of a frozen species i due to heavy cosmic rays and $\phi_{\rm HCR}$ is the average heavy-ion cosmic ray flux (ions cm^{-2} s^{-1}). The half-life, $t_{1/2}$, of a given species i may be obtained from Eq. (16) by writing

$$t_{1/2,i} = \frac{\ln 2}{R_i} \quad [{\rm s}], \tag{17}$$

which does not depend on the molecular number density in the ice. The dissociation cross-section depends on the projectile energy: for Ni ions, $\sigma_{{\rm d},i}$ is typically 2×10^{-13} cm^2 at 46 MeV, decreasing to 0.3×10^{-13} cm^2 at 537 MeV (Seperuelo Duarte et al. 2009b). Nevertheless, assuming the values of $\sigma_{{\rm d},i}$ for Ni ions at 46 MeV as the average value and $\phi_{\rm HCR} \sim 5 \times 10^{-2}$ ions cm^{-2} s^{-1} as the heavy-ion cosmic ray flux, R can be estimated.

Table 5 presents the average dissociation rate and the half-lives of water, ammonia, and CO molecules bombarded by heavy ions. The estimated half-life of the studied species for a typical heavy cosmic ray flux is about 2–3 $\times$ 10^6 years. This value is in a good agreement with the half-lives of typical molecular clouds and protostellar clouds (e.g., Millar & Nejad 1985; Takeuchi et al. 2005). More reliable estimation of molecular dissociation rates and half-lives promoted by the direct impact of heavy cosmic rays on interstellar ices depends on more accurate measurements and determinations of the average heavy-ion cosmic-ray flux inside these dense environments.

5. Summary and conclusions

We have performed an experimental study of the interaction of heavy, highly charged and energetic ions (46 MeV $^{58}Ni^{13+}$) with ammonia-containing ices H_2O:NH_3 (1:0.5) and H_2O:NH_3:CO (1:0.6:0.4) to simulate the physical chemistry induced by cosmic rays inside dense regions of the interstellar medium such as dense molecular clouds or protoplanetary disks. Our conclusions are:

1. At the beginning of the irradiation, the ices become compact as indicated by the particular dependence of the column density on the fluence. Measuring the degree of compaction through the integrated area of the OH dangling bond feature (~3650 cm^{-1}) of water molecules trapped into ice micropores, the of the impact of heavy ions seems to be at least 3 orders of magnitude higher than the effect of (0.8 MeV) protons.
2. The infrared spectra of the irradiated samples indicate the production of several new species, including OCN^-, HNCO, and NH_4^+. The OCN^- band (2169 cm^{-1}) is observed even at room temperature. During the ice heating, a broad feature was observed around 2218–2200 cm^{-1} and was tentatively assigned to non-volatile nitriles. At room temperature, an intense and sharp feature was observed at ~2150 cm^{-1} and was tentatively assigned to aliphatic isocyanide ~2150 cm^{-1}.
3. The spectra of the irradiated H_2O:NH_3:CO ice (1:0.6:0.4) at room temperature contain several bands, which are tentatively assigned to zwitterionic glycine and HMT. The

presence of these complex molecules in the organic residue produced by the bombardments of interstellar ice analogs by energetic and heavy ions, has to be confirmed.

4. The measured value for the dissociation cross-section of water, ammonia, and carbon monoxide (in the tertiary mixture ice) due to heavy cosmic ray analogs are $\sim 2 \times 10^{-13}$, 1.4×10^{-13}, and 1.9×10^{-13} cm^2, respectively. These values do not seem to be affected by small (<30%) changes in the initial relative molecular abundances.
5. In the presence of a typical heavy-ion cosmic ray field, the estimated half-lives of the studied species is about $2-3 \times 10^6$ years. This value is in a good agreement with the half-lives of typical molecular clouds and protostellar clouds.

Although they represent only a small fraction (~1%) of the cosmic-ray flux, some effects (e.g., molecular sputtering and ice compaction) caused by heavy ions on interstellar ice grains are more intense than those caused by protons. This should be taken into consideration in future chemical models of inner regions of molecular clouds since heavy ions will contribute molecules to the gas phase and trigger chemical surface and bulk reactions.

Acknowledgements. The authors acknowledge the agencies COFECUB (France) as well as CAPES, CNPq and FAPERJ (Brazil) for partial support. We thanks Th. Been, I. Monnet, Y. Ngono-Ravache for technical support, and D. P. P. Andrade for fruitful discussions. We would like to express our sincere gratitude to the anonymous referee for some very valuable input and suggestions.

References

Andrade, D. P. P., Boechat-Roberty, H. M., da Silveira, E. F., et al. 2008, J. Phys. Chem. C., 112, 11954
Bernstein, M. P., Dworkin, J. P., Sandford, S. A., et al. 2002, Nature, 416, 401
Bernstein, M. P., Sandford, S. A., & Allamandola, L. J. 2000, ApJ, 542, 894
Bird, M. K., Janardhan, P., Wilson, T. L., et al. 1997, Earth Moon Planets, 78, 21
Boogert, A. C. A., Pontoppidan, K. M., Lahuis, F., et al. 2004, ApJS, 154, 359
Brown, W. L., Lanzerotti, L. J., & Johnson, R. E. 1982, Science, 218, 525
Brown, W. L., Augustyniak, W. M., Marcantonio, K. J., et al. 1984, Nucl. Instr. Meth. B1, IV, 307
Chokshi, A., Tielens, A. G. G. M., & Hollenbach, D. 1993, ApJ, 407, 806
Collings, M. P., Anderson, M. A., Chen, R., et al. 2004, MNRAS, 354, 1133
Chan, W. F., Cooper, G., & Brion, C. E. 1993, Chem. Phys. 178, 387
Chiar, J. E., Tielens, A. G. G. M., Whittet, D. C. B., et al. 2000, ApJ, 537, 749
Chiar, J. E., Adamson, A. J., Pendleton, Y. J., et al. 2002, ApJ, 570, 198
Chen, Y.-J., Nuevp, M., Yih, T.-S., et al. 2008, MNRAS, 384, 605
Demyk, K., Dartois, E., d'Hendecourt, L., et al. 1998, A&A, 339, 553
Drury, L. O. C., Meyer, J.-P., & Ellison, D. C. 1999, Topics in Cosmic-Ray Astrophysics, ed. M. A. DuVernois (New-York: Nova Science Publishers)
Ehrenfreund, P., & Charnley, S. B. 2000, ARA&A, 38, 427
Ehrenfreund, P., & Shuttle, W. A. 2000, From molecular clouds to planetary system, Proc. IAU Symp., 197
Elsila, J. E., Dworkin, J. P., Bernstein, M. P. Martin, M. P., & Sandford, S. A. 2007, ApJ, 660, 911
Famá M., Shi, J., & Baragiola, R. A. 2008, Surface Sci., 602, 156
Gerakines, P. A., Scutte, W. A., Greenberg, J. M., et al. 1995, A&A, 296, 810
Gibb, E. L., Whittet, D. C. B., Schutte, W. A., et al. 2000, ApJ, 536, 347
Gibb, E. L., Whittet, D. C. B., Boogert, A. C. A. 2004, ApJSS, 151, 35
Gibb, E. L., Whittet, D. C. B., & Chiar, J. E. 2001, ApJ, 558, 702
Gomis, O., Leto, G., & Strazulla, G., 2004a, A&A, 420, 405
Gomis, O., Satorre, M. A., Strazulla, G., et al. 2004b, Plan. Spac. Sci. 52, 371
Grim, R. J. A., & Greenberg, J. M. 1987, ApJ, 321, L91
Grün, E., Gustafson, B., Mann, I., et al. 1994, A&A, 286, 915
d'Hendecourt, L. B., & Allamandola, L. J. 1986, A&ASS, 64, 453
d'Hendecourt, L. B., Alamandola, L. J., & Greenberg, J. M. 1985, A&A, 152, 130
Holtom, P. D., Bennett, C. J., Osamura, Y., Mason, N. J., & Kaiser, R. I. 2005, ApJ, 626, 940
Hudson, R. L., & Moore, M. H. 2000, A&A, 357, 787
Hudson, R. L., & Moore, M. H. 2002, ApJ, 568, 1095
Hudson, R. L., Moore, M. H., & Gerakines, P. A. 2001, ApJ, 550, 1140
Imanaka, H., Khare, B. N., Elsila, J. E., et al. 2004, Icarus, 168, 344
Iza, P., Farenzena, L. S., Jalowy, T., et al. 2006, Nucl. Instr. Meth. Phys. Res. B, 245, 61
Jamieson, C. S., Bennett, C. J., Mebel, A. M., et al. 2005, ApJ, 624, 436
Jenniskens, P., Blake, D. F., & Kouchi A. 1998, Solar System Ices, ed. B. Schmitt, C. de Bergh, & M. Festou, Astrophys. and Space Sci. Libr. (Kluwer Academic Press), 139
Keane, J. V., Tielens, A. G. G. M., Boogert, A. C. A., Schutte, W. A., & Whittet, D. C. B. 2001, A&A, 376, 254
Kawakita, H., Dello Russo, N., Furusho, R., et al. 2006, ApJ, 643, 1337
Kerkhof, O., Schutte, W. A., & Ehrenfreund, P. 1999, A&A, 346, 990
Kobayashi, K., Kaneko, T., Takano, Y. et al. 2008, Proc. IAU Symp. 251, 465
Lacy, J. H., Baas, F., Allamandola, L. J., et al. 1984, ApJ, 276, 533
Lacy, J. H., Faraji, H., Sandford, S. A., et al. 1998, ApJ, 501, L105
Lafosse, A., Bertin, M., Domaracka, A., et al. 2006, Phys. Chem. Chem. Phys., 8, 5564
Léger, A., Jura, M., & Omont, A. 1985, A&A, 144, 147
Li, A., & Greenberg, J. M. 1997, A&A, 323
Loeffler, M. J., Raut, U., Vidal, R. A., Baragiola, R. A., & Carlson, R. W. 2006, Icarus, 180, 265
Mathis, J. S. 1990, ARA&A, 28, 37
Mathis, J. S., Rumpl, W., & Nordsieck, K. H. 1977, ApJ, 217, 105
McLaren, R., Ishii, I., Hitchcock, A. P., et al. 1987, J. Chem. Phys., 87, 4344
Moore, M. H., Donn, B., Khanna, R. et al. 1983, et al. 1983, Icarus, 54, 388
Moore, M. H., Ferrante, R. F., Hudson, R. L., et al. 2007, Icarus, 190, 260
Mennella, V., Baratta, G. A., Esposito, A., Ferini, G. & Pendleton, Y. J. 2003, ApJ, 587, 727
Millar, T. J., & Nejad, L. A. M. 1985, MNRAS, 217, 507
Morfill, G. E., Volk, H. J., & Lee, M. A. 1976, J. Geophys. Res., 81, 5841
Muñoz Caron, G. M., & Shutte, S. A. 2003, A&A, 412, 121
Muñoz Caro, G. M., Meierhenrich, U. J., Schutte, W. A., et al. 2002, Nature, 416, 403
Nastasi, M., Mayer, J., & Hirvonen, J. K. 1996, in Ion-Solid Interactions: Fundamentals and Applications, Cambridge Solid State Science Series, (Cambridge University Press)
Novozamsky, J. H., Schutte, W. A., & Keane, J. V. 2001, A&A, 379, 588
Nuevo, M., Meierhenrich, U. J., Muñoz Caro, G. M., et al., 2006, A&A, 457, 741
Nuevo, M., Meierhenrich, U. J., D'Hendecourt, L., et al. 2007, Adv. Space Res., 39, 400
Palumbo, M. E. 2006, A&A, 453, 903
Palumbo, M. E., Strazulla, G., Pendleton, Y. J., et al. 2000, ApJ, 534, 801
Pontoppidan, K. M., Dartois, E., van Dishoeck, E. F., Thi, W.-F., & d'Hedencourt, L. 2003, A&A, 404, L17
Prasad, S. S., & Tarafdar, S. P. 1983, ApJ, 267, 603
Pendleton, Y. J., Tielens, A. G. G. M., Tokunaga, A. T., et al. 1999, ApJ, 475, 144
Roberts, J. F., Rawlings, J. M. C., Viti, S., et al. 2007, MNRAS, 382, 733
Rowland, B., & Devlin, J. P. 1991, J. Chem. Phys., 94, 812
Rowland, B., Fisher, M., & Devlin, J. P. 1991, J. Chem. Phys., 95, 1378
Raunier, S., Chiavassa, T., Marinelli, F., Allouche, A., & Aycard, J. P. 2003, J. Phys. Chem. A, 107, 9335
Schutte, W. A., & Greenberg, J. M. 1997, A&A, 317, L43
Shen, C. J., Greenberg, J. M., Schute, W. A., et al. 2004, A&A, 415, 203
Seperuelo Duarte, E., Boduch, P., Rothard, H., et al., 2009a, A&A, 502, 599
Seperuelo Duarte, E., Boduch, P., Rothard, H., Been, T., Dartois, E., et al. 2009b, A&A, submitted
Schmidt, R., Schoppmann, C., Brandle, D., et al. 1991, Phys. Rev. B, 44, 2
Soifer, B. T., Puetter, R. C., Russell, R. W., et al. 1979, ApJ, 232, L53
Spoon, H. W. W., Moorwood, A. F. M., Pontoppidan, K. M., et al. 2003, A&A, 402, 499
Takano, Y., Takahashi, J.-I., Kaneko, T., Marumo, K., & Kobayashi, K. 2007, Earth and Planetary Sci. Lett., 254, 106
Takeuchi, T., Clarke, C. J., & Lin, D. N. C. 2005, ApJ, 627, 286
Taylor, A. D., Baggaley, W. J., & Steel, D. I. 1996, Nature, 380, 323
Tegler, S. C., Weintraub, D. A., Allamandola, L. J., et al. 1993, ApJ, 411, 260
Tielens, A. G. G. M., & Hagen, W. 1982, A&A, 114, 245
van Broekhuizen, F. A., Keane, J. V., & Schutte, W. A. 2004, A&A, 415, 425
van Broekhuizen, F. A., Pontoppidan, K. M., Fraser, H. J. et al. 2005, A&A, 441, 249
Wang, F., Larkins, F. P., Brunger, M. J., Michalewicz, M. T., & Winkler, D. A. 2001, Spectrochimica Acta A, 57, 9
Witt, A. N., Smith, R. K., & Dwek E. 2001, ApJ, 550, L201
Whittet, D. C. B., Pendleton, Y. J., Gibb E. L., et al. ApJ, 2001, 550, 793